International Journal of Applied Electromagnetics and Mechanics 69 (2022) 139–147
DOI 10.3233/JAE-210183
IOS Press

Study of magnetic force excitations in salient pole synchronous generators considering geometrical modifications by conformal mapping

Kevin Jansen*, Alexander Kern, Christoph Mülder and Kay Hameyer
Institute of Electrical Machines (IEM), RWTH Aachen University, Aachen, Germany

Abstract. The simulation of electrical machines at the first design stage requires efficient methods to characterize among other properties its vibrational behavior. Particularly when considering both designed and parasitic geometrical modifications, magnetic circuit calculations of large-dimensioned machines by finite-element methods (FEM) are cumbersome. Semi-analytical approaches by means of conformal mapping are therefore useful to estimate the impact of several effects, such as asymmetric stator laminations, rotor pole shapes and air gap imperfections. No-load operation is studied and the presented approach is validated by FEM simulations. The aim of this work is to study force excitations by the magnetic air gap field in salient multi-pole synchronous generators deviating from ideal and symmetrical geometrical conditions by using conformal maps.

Keywords: Parasitic magnetic forces, conformal mapping, electrical machines, large drives

AUTHOR COPY

1. Introduction

Regulatory requirements for the noise emission of decentralized energy producers, as e.g. wind energy converters, steadily increase. Tonal noises excited by the magnetic air gap field of generators are therefore criteria, which have to be considered in the design process. At an early stage, the impact of geometrical changes, which are both intended to mitigate field harmonics and occur parasitically due to rotor misalignment, are in the focus. Since numerical calculation based on finite element analysis of multi-pole machine topologies are time-consuming, semi-analytical approaches using conformal maps are appropriate to study several geometrical conditions, which can occur at the air gap of the generator. These methods have already been applied to non-salient permanent magnet excited machines and validated by finite element simulations [1,2].

In this work, the magnetic air gap field and forces of an electrically-excited salient pole synchronous generator are studied by conformal maps in contrast to other work using analytical formulas, which are limited to idealized [3] or other geometries [4].

After describing the basic methodology of conformal mapping, the modeling approach for geometries with non-cylindrical air gap shapes is presented. The mapping of two geometrical modifications, that are sine pole rotors and anomalous stator laminations with double teeth and slots, is presented. The magnetic

*Corresponding author: Kevin Jansen, Institute of Electrical Machines (IEM), RWTH Aachen University, Schinkelstraße 4, 52062 Aachen, Germany. Tel.: +49 241 8090258; E-mail: kevin.jansen@iem.rwth-aachen.de.

1383-5416/$35.00 © 2022 – IOS Press. All rights reserved

air gap flux density distributions and radial force density orders occurring in these topologies are analyzed and compared to finite element method (FEM) based simulations. Finally, the conclusions are drawn and an outlook for further research work is given.

2. Methodology

A Schwarz–Christoffel conformal mapping (CM) approach is applied for the impact analysis of non-uniform air gap shapes due to sine pole as well as double tooth and double slot configurations on the magnetic air gap flux density and radial force density. The 2D polygon describing the machine geometry is mapped to a regular annulus. Applying the inverse transformation to the flux density solution in the annulus yields the magnetic flux density in the original geometry.

2.1. Magnetic flux density calculation by conformal maps

In previous works [1,4], machine geometries are modeled by defining the vertices of the geometry polygon as complex numbers s of the form

$$s = Re^{j\alpha}, \tag{1}$$

where R and α are the radius from the center of origin and the angle of the vertex from the horizontal axis, respectively. Schwarz–Christoffel mapping does not allow the geometry edges to have a curved shape. Therefore, the defined geometry is transformed to the rectified z-plane using

$$z = \ln(s) = \ln(R) + j\alpha \tag{2}$$

as presented in [1]. Hence, only geometrical contours, which are circle arcs with center points coinciding with the center of origin and lines with strictly radial orientation, can be accurately modeled with this approach. Instead of only modeling the vertices of the geometry, the configuration is approximated by a polygon of N sample points along the edges of the target geometry in this work. The impact of this approximation on the accuracy of results is studied. The rectified geometry is transformed to a rectangular domain using Schwarz–Christoffel mapping as presented in [5].

This rectangular w-plane is mapped to the ψ-plane of a regular annulus as presented in [6] and the flux density solution $\underline{B}_\psi$ in the regular annulus is calculated [7]. The flux density $\underline{B}_s$ in the s-plane is calculated by [1]:

$$\underline{B}_s = \underline{\lambda}^* \cdot \underline{B}_\psi. \tag{3}$$

The complex relative permeance function $\underline{\lambda}$ is calculated from the product of the partial derivatives of the transformation functions:

$$\underline{\lambda} = \left(\frac{\partial z}{\partial s} \frac{\partial w}{\partial z} \frac{\partial \psi}{\partial w} \right) \cdot \frac{1}{\lambda_0}. \tag{4}$$

The real valued relative permeance function λ_0 is calculated by mapping a slotless reference geometry in the s-plane to a regular annulus in the ψ plane in order to cancel the impact of the transformation on the resulting complex permeance function. The permeance functions for the rotor and stator are derived separately and superposed to the relative air gap permeance $\underline{\lambda}_{\mathrm{AG}}$:

$$\underline{\lambda}_{\mathrm{AG}} = \underline{\lambda}_{\mathrm{Stator}} \cdot \underline{\lambda}_{\mathrm{Rotor}}. \tag{5}$$

AUTHOR COPY

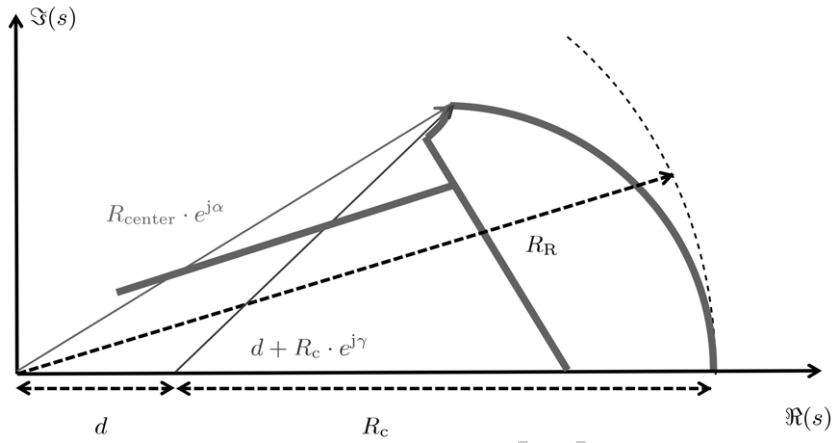

Fig. 1. Schematic representation of the sine pole rotor geometry in the s-plane.

The relative rotor and stator permeance functions are calculated for different combinations of a sine pole rotor geometry, a double tooth and double slot configuration as well as their regular counterparts.

2.2. *Sine pole geometry*

When compared to a cylindrical rotor pole design, the sinusoidally shaped pole shoes are used in order to suppress higher harmonics in the magnetic air gap flux density [8]. The specific radius of curvature is a design parameter so that in rated operation the first harmonic of the air gap magnetic flux density is approximately its amplitude:

$$^{1}\boldsymbol{B}_{\delta} \approx \boldsymbol{B}_{\delta}. \tag{6}$$

In Fig. 1, the sine pole rotor geometry in the s-plane is illustrated schematically. The dashed circle arc indicates the outer contour of a cylindrically shaped rotor pole geometry. In this case, all points along the pole surface have an equal distance R_R from the center of the machine. For a sine pole rotor shape, the air gap width varies along the surface of the pole depending on the specific radius of curvature R_c and arc angles γ. Hence, points along its surface are described by a circle that has an origin shifted by d from the center of the machine.

The following transformations are deduced in order to apply Schwarz–Christoffel mapping correctly for the considered curved geometry:

$$\alpha = \arctan\left(\frac{R_c \cdot \sin(\gamma)}{d + R_c \cdot \cos(\gamma)}\right) \tag{7}$$

and

$$R_{\text{center}} = R_c \cdot \frac{\sin(\gamma)}{\sin(\alpha)}. \tag{8}$$

The necessary amount of discretization points N along the rotor surface is studied and the implications on the resulting magnetic flux and force density distributions in the air gap are evaluated.

AUTHOR COPY

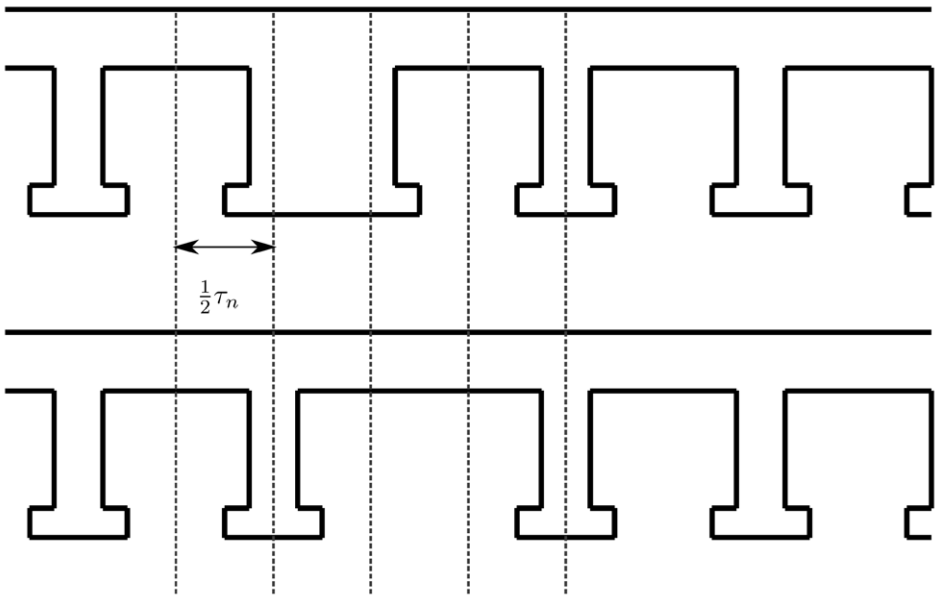

Fig. 2. Schematic representation of the double tooth and double slot stator geometry.

2.3. Double tooth and double slot stator topology

The insertion of a double tooth and a double slot in a uniformly slotted stator geometry is a concept of stator shifting in order to reduce high order harmonic content of the air gap magnetic flux density and the resulting magnetic force excitations [9,10]. The double tooth and the double slot occur at a fixed number of uniform stator slots in each of a symmetrical unit that is one eighth of the circumference. In each symmetrical unit the stator permeance functions describing the original and the modified stator geometry have a spatial phase shift of half a slot pitch between the double tooth and the double slot. In Fig. 2, the concept of this stator configuration is illustrated schematically. The dashed lines indicate the circumferential width of a half slot pitch.

2.4. Magnetic force densities

The electromagnetic air gap force density in radial direction σ_{rad} can be derived from the Maxwell stress tensor on the basis of the radial and tangential components of the magnetic air gap flux density [11]:

$$\sigma_{\text{rad}}(\alpha, t) = \frac{B_{\delta,\text{rad}}(\alpha, t)^2 - B_{\delta,\text{tan}}(\alpha, t)^2}{2\mu_0}. \tag{9}$$

Analogously to the air gap magnetic flux density, the force excitations are a function of the time instant and the circumferential position. Therefore, a 2D-Fast-Fourier transformation (2D-FFT) is applied in order to analyze the electromagnetic force excitation in the frequency and spatial domain. Hereby, a magnetically excited force wave propagates along the circumference of the machine with a shape correlating with the spatial order η and a frequency correlating with the temporal order ν.

AUTHOR C

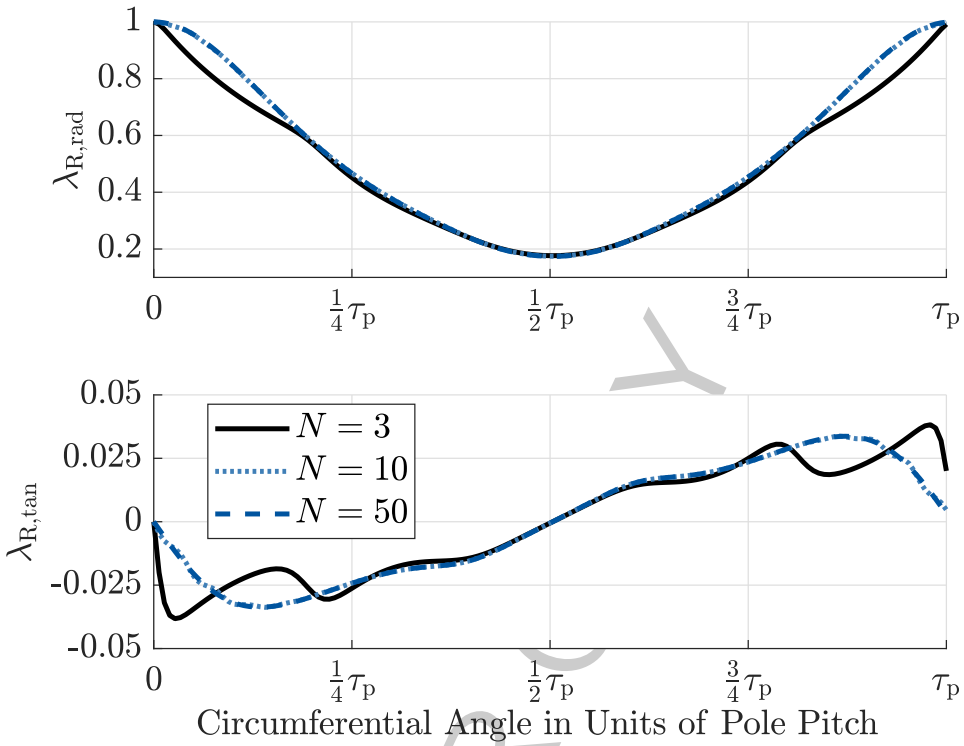

Fig. 3. Comparison of the radial and tangential rotor permeance function over one symmetrical unit of a pole pitch as a function of the number of discretization grid points N.

In the following sections, these order pairs are indicated as tuples of the form $(\frac{\nu}{p}, \eta)$, where p is the pole pair number of the machine.

3. Results

3.1. Sine pole rotor

In Fig. 3, the radial and tangential components of the geometry of the sine pole permeance function are illustrated for varying numbers of discretization points N along the curvature of the pole. The number of discretization points affects the shape of the resulting radial and tangential rotor permeance function significantly. A number of $N > 10$ grid points is necessary in order to avoid discontinuities in the derivatives of the transformation functions. The modeling accuracy converges for a further increase of the discretization grid points.

In Fig. 4, the comparison of the magnetic air gap flux densities calculated by the conformal mapping approach and FEM is illustrated at no-load operation. For validation purposes the operating point is chosen in such a way that the lamination material has linear magnetic behavior, as the conformal mapping approach does not consider magnetic saturation. The finite-element model used for validation is illustrated in [12]. The rotor pole shape is approximated with $N = 10$ discretization points. The flux density distribution calculated from CM matches the FE solution. The sinusoidal rotor surface leads to

AUTHOR COPY

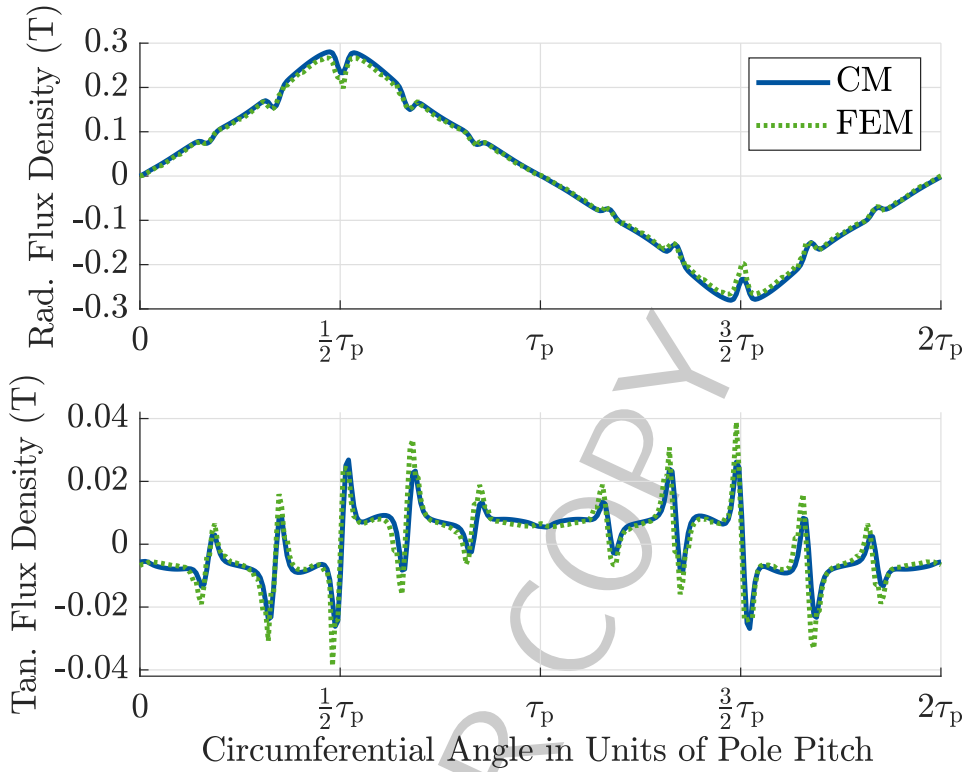

Fig. 4. Comparison of the radial and tangential component of the air gap magnetic flux density at no-load operation.

a magnetic flux density distribution of sinusoidal shape. The stator slotting locally decreases the radial magnetic flux density and increases the tangential flux density.

In order to quantify force excitations, radial force density distributions are considered. In Fig. 5, the radial force excitations are illustrated after a 2D-FFT. As the pole number of the machine is 96, spatial orders which are multiples of 96 are primarily excited.

3.2. Double slot and double tooth topology

In Fig. 6 the relative air gap permeance functions across multiple slot pitches τ_n are illustrated for the double stator slot and double tooth topology. Across the regular slot pitches, the permeance function matches the behavior of a regular stator geometry. The presence of a double slot leads to an increase of tangential magnetic flux and decrease of radial magnetic flux at the wider slot opening. For the double tooth an extension of the area, where the permeance function is of constant value, is observed.

In Fig. 7, the radial force density spectrum of the topology with both sine pole rotor and double slot and double tooth stator is illustrated in the frequency domain. Due to the double tooth and double slot configuration occurring eight times over the circumference of the machine, radial force waves with spatial orders, which are multiples of eight, are additionally excited. Excitations with low frequency orders and low spatial orders such as (2, 0), (4, 0), (6, 0) and (8, 0) occur with an increased amplitude. High frequency orders with low spatial orders such as the slot harmonics (12, 0) and (24, 0) are reduced. As expected, the stator configuration shifts magnetic force excitations towards lower frequencies.

AUTHOR COPY

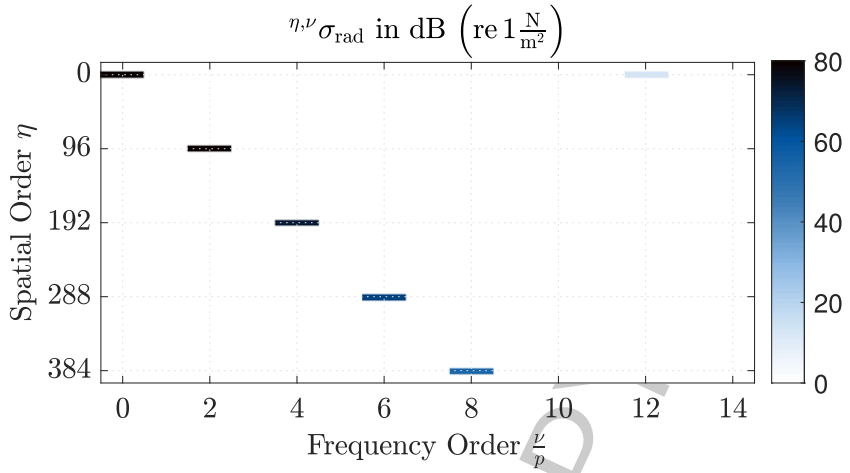

Fig. 5. Radial force density spectrum for a sine pole geometry at no-load operation.

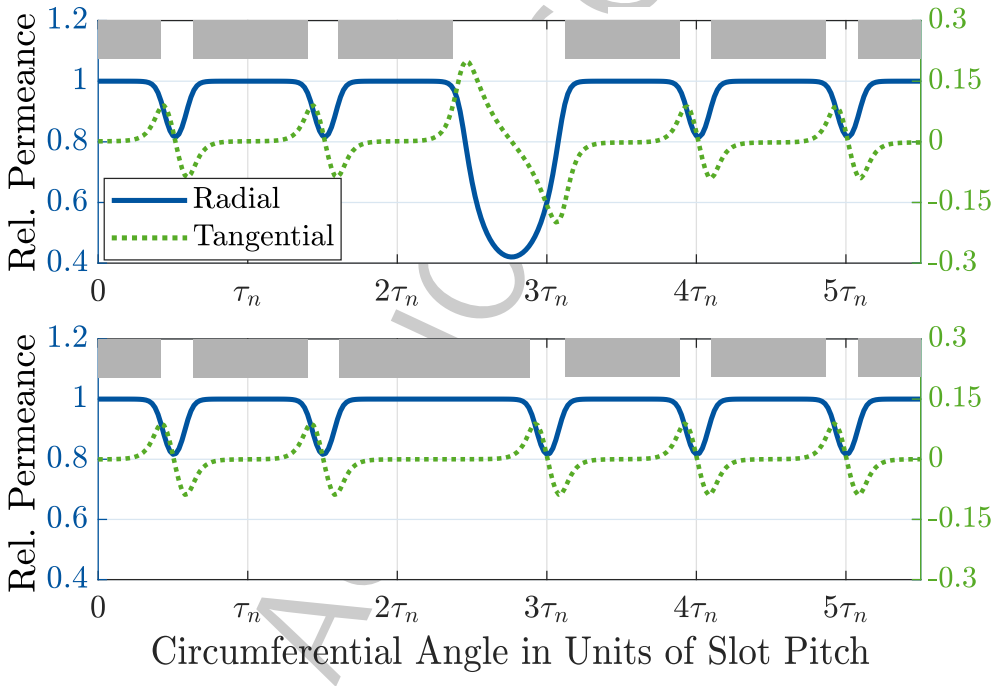

Fig. 6. Radial and tangential relative permeance components of the double slot and double tooth topology.

4. Conclusion and outlook

The magnetic air gap flux density solution of a sine pole rotor geometry at no-load operation is calculated by means of a conformal mapping approach and validated by the FEM. The impact of discretization in the modeling of the geometry is studied and a sufficient amount of sample points is determined. The relative air gap permeance resulting from doubled stator slots and teeth used in stator

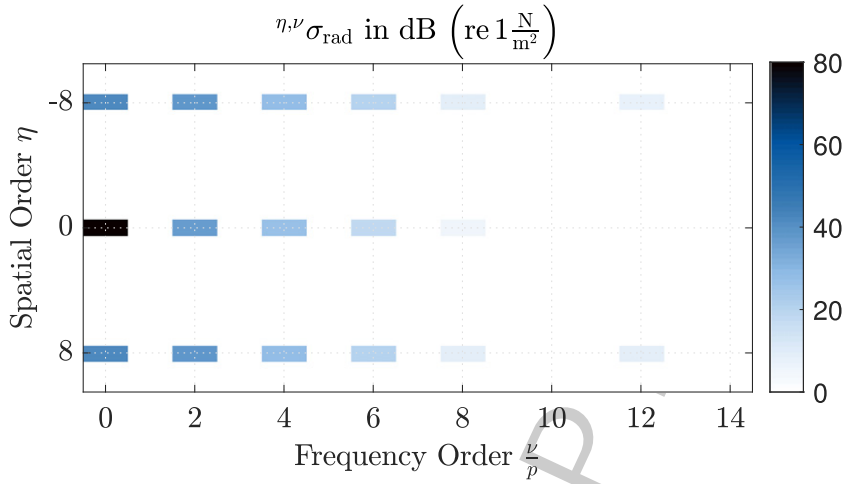

Fig. 7. Radial force density spectrum for a double slot and double tooth configuration at no-load operation.

shifting are presented. The radial force excitation resulting from stator shifting is calculated and the impacts on the resulting space and frequency orders are discussed. The presented double tooth and double slot topology shifts magnetic force excitations towards lower frequencies.

In future work, this conformal mapping approach is used to model further air gap imperfections such as rotor ovalization and eccentricities and evaluate electromagnetically excited forces and their impact on acoustic behavior.

AUTHOR COPY

References

[1] K. Boughrara, R. Ibtiouen, D. Zarko, O. Touhami and A. Rezzoug, Magnetic field analysis of external rotor permanent-magnet synchronous motors using conformal mapping, *IEEE Transactions on Magnetics* **46**(9) (2010), 3684–3693.

[2] A. Hanic, D. Zarko and Z. Hanic, A novel method for no-load magnetic field analysis of saturated surface permanent-magnet machines using conformal mapping and magnetic equivalent circuits, *IEEE Transactions on Energy Conversion* **31**(2) (2016), 740–749.

[3] O. Misir, F. Dobbert and B. Ponick, Analytical method for the air gap permeance calculation of salient pole synchronous machines, *e & i Elektrotechnik und Informationstechnik* **133**(2) (2016), 103–111.

[4] A. Tikellaline, K. Boughrara and N. Takorabet, Magnetic field analysis of double excited synchronous motor using numerical conformal mapping, in: *2017 5th International Conference on Electrical Engineering – Boumerdes (ICEE-B)*, IEEE, 2017, pp. 1–6.

[5] T.A. Driscoll and L.N. Trefethen, Schwarz–Christoffel mapping, in: *Cambridge Monographs on Applied and Computational Mathematics*, Vol. 8, Cambridge University Press, Cambridge, 2002.

[6] M. Schröder, A. Ruf, D. Franck and K. Hameyer, Einfluss von parasitären effekten und fertigungsabweichungen auf die kräfte in elektrischen maschinen, *e & i Elektrotechnik und Informationstechnik* **134**(2) (2017), 127–138.

[7] B. Hague, *The Principles of Electromagnetism Applied to Electrical Machines: (Formerly Titled: Electromagnetic Problems in Electrical Engineering)*, Dover Publications, 1962.

[8] S.A. Evans, Salient pole shoe shapes of interior permanent magnet synchronous machines, in: *The XIX International Conference on Electrical Machines – ICEM 2010*, 2010, pp. 1–6.

[9] P.B. Reddy, K.-K. Huh and A.M. El-Refaie, Generalized approach of stator shifting in interior permanent-magnet machines equipped with fractional-slot concentrated windings, *IEEE Transactions on Industrial Electronics* **61**(9) (2014), 5035–5046.

[10] A.S. Abdel-Khalik, S. Ahmed and A. Massoud, Application of stator shifting to five-phase fractional-slot concentrated winding interior permanent magnet synchronous machine, *IET Electric Power Applications* **10**(7) (2016), 681–690.

[11] M. Schröder, D. Franck and K. Hameyer, Analytical modeling of manufacturing tolerances for surface mounted permanent magnet synchronous machines, in: *2015 IEEE International Electric Machines & Drives Conference (IEMDC)*, 2015, pp. 1138–1144.
[12] C. Mülder, F. Müller, A. Thul, K. Hameyer and C. Meier, Electromagnetic study of direct-driven wind turbine generators by coupled field-circuit simulations and full-scale bench tests, in: *2021 IEEE Energy Conversion Congress and Exposition (ECCE)*, IEEE, 2021, pp. 422–429.

AUTHOR COPY